Chiral Nanoparticle as a New Efficient Antimicrobial Nanoagent

Qi Xin, Qian Liu, Lingling Geng, Qiaojun Fang, and Jian Ru Gong**

The global spread of bacterial resistance to currently available antibiotics poses a serious threat to public health and underscores an urgent need for new alternative antimicrobial agents.[1] The rapid development of nanoscience and technology greatly benefits the infectious disease management.[2] Owing to superior features such as increased membrane permeability and lack of efflux pump compared with traditional antibiotics, a series of antimicrobial nanoparticles (NPs) such as nanocarbon,[3] cationic conjugated polymers,[4] peptide hydrogels,[5] semiconductor, and noble-metal NPs[6] possess strong antimicrobial activity and are less prone to induce bacterial resistance. Nevertheless, most of them have little selective toxicity[2b,7]—an indispensable characteristic of an ideal antimicrobial agent, which will hinder further antimicrobial applications. Therefore, it is highly desirable to seek novel NPs with efficient antimicrobial activity and high selective toxicity.

Specifically functionalized NPs can selectively bind biological targets,[8] which will provide an opportunity for developing novel antimicrobial NPs to address the issue of low selective toxicity. Chiral molecular recognition is an effective way of binding.[9] Among the chiral molecules, the biomolecule D-glutamic acid (D-Glu) is unique because it is an essential substance for synthesis of peptidoglycan (PG)—a vital component of bacterial cell wall rather than of mammalian cells—which protects bacteria from destruction by high internal osmotic pressure.[10] Thus, disruption of the PG biosynthesis by inhibiting the D-Glu associated catalytic step can be utilized to eliminate bacteria while leaving mammalian cells intact. Addition of D-Glu as an important cytoplasmic synthetic step of PG is catalyzed by MurD ligase (**Scheme 1**). Based on the "lock and key" principle in enzyme catalysis,[11] MurD ligase possesses high stereochemical selection for its D-Glu substrate. Thus, the derivative of D-Glu has been a widely used starting point in design of MurD-based inhibitors which exert different degrees of inhibition effect.[12] However, none of these MurD ligase inhibitors so far has yet achieved success for production of therapeutic antimicrobial agents due in large part to the difficulties in penetrating the dense outer membrane into bacterial cytoplasm to affect the activity of MurD.[13] Also, the efflux pump commonly existed in bacteria might lead to the ineffectiveness of these inhibitors.[14]

Here, we propose the design of a novel D-Glu functionalized NP targeting toward MurD ligase to achieve efficient antimicrobial activity and high selective toxicity. In this study, the emerging graphene quantum dot (GQD) was selected as a model NP. GQD, generally referring to a kind of quasi-zero-dimensional NPs with a honeycomb network of sp^2-hybridized carbon atom at the central region and oxygen-containing functional groups mainly attached to the carbon atoms at the edge, arouses enormous research interests in biomedical fields because of its excellent properties such as superior long-term biosafety, tunable fluorescence emission, and excellent photostability against photobleaching and blinking, as well as the low cost and simplicity of synthesis.[15] Though GQD is inactive against bacteria, its oxygen-containing groups especially carboxyl can facilitate its modification with functional molecules,[16] thus imparting antimicrobial potential to it. Our experimental studies reveal that the obtained D-Glu-functionalized GQD (DGG) can penetrate the bacterial cell membrane and specifically bind to cytoplasmic MurD to inhibit its catalyzing activity in the intracellular PG biosynthesis, resulting in damage of the cell wall, subsequent leakage of cytoplasmic contents, and final killing of bacteria (Scheme 1). Considering the lack of endogenously produced D-Glu and related enzymes in mammalian cells, DGG hardly targets mammalian proteins to affect their functions, thus being harmless to mammalian cells during the bactericidal process. In contrast, L-Glu-functionalized GQD (LGG) shows a negligible influence on both bacteria and mammalian cells. Further theoretical calculation results show that there is a significant difference in the binding ability between DGG/MurD and LGG/MurD, suggesting that the chiral structure of antimicrobial NPs plays an important role in their biological activity.

DGG/LGG was prepared by a facile one-pot pyrolysis reaction using citric acid as a precursor with addition of D-Glu/L-Glu. The Glu group conjugates with the central graphene domain via amide bond and remains stable (Figures S1 and S2 in the Supporting Information). For comparison, unfunctionalized GQD (UG) was also synthesized under the same experimental conditions as those used for DGG/LGG, except without adding D-Glu/L-Glu. The as-prepared DGGs are uniform and well dispersed with an average lateral size of 3 nm (**Figure 1**a,b), and mainly consist of monolayer graphene sheets (Figure S3, Supporting Information). The high-resolution transmission electron microscopy image shows an in-plane lattice spacing of 0.214 nm in DGG, corresponding well to the (100) facet of

Dr. Q. Xin, Dr. Q. Liu, Prof. J. R. Gong
CAS Center of Excellence for Nanoscience
CAS Key Laboratory for Nanosystem and Hierarchical Fabrication
National Center for Nanoscience and Technology
11 Beiyitiao Zhongguancun
Beijing 100190, P. R. China
E-mail: gongjr@nanoctr.cn
Dr. L. Geng, Prof. Q. Fang
CAS Key Laboratory for Biological Effects of Nanomaterials and Nanosafety
National Center for Nanoscience and Technology
11 Beiyitiao Zhongguancun, Beijing 100190, P. R. China
E-mail: fangqj@nanoctr.cn

DOI: 10.1002/adhm.201601011

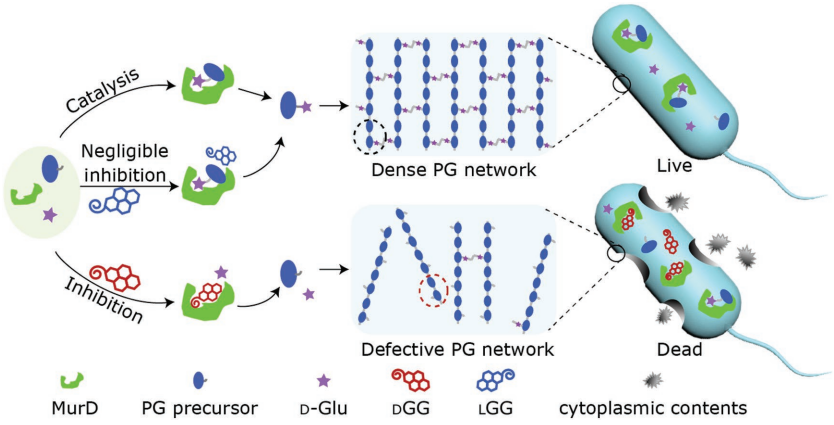

Scheme 1. The antimicrobial strategy of chiral NPs. Under the normal growth condition, MurD ligase catalyzes the intracellular addition of D-Glu onto the cytoplasmic PG precursor. By consecutive addition of other three amino acids and glycosyl transfer, the PG monomer with a complete peptide side chain (black dashed circle) is synthesized and then the peptide side chains of PG monomers cross-link directly to form a dense PG network. In our work, DGG can bind to MurD protein through occupying the active sites for D-Glu substrate owing to the favorable steric match. Thus, the catalytic activity of MurD is inhibited and successive addition of other amino acids to form peptide side chains is also blocked. After glycosyl transfer, only the PG monomer with an incomplete peptide side chain (red dashed circle) is produced and the subsequent cross-link process is disrupted, forming a defective PG network which causes leakage of cytoplasmic contents and final killing of bacteria. In contrast, LGG shows a negligible influence on the catalytic activity of MurD and displays little antimicrobial activity.

graphene (inset I of Figure 1a).[17] The related fast fourier transform (FFT) and reverse FFT pattern display a hexagonal crystalline structure in the central region of DGG (insets II and III of Figure 1a). The similar morphology and structure were observed for LGG and UG (data not shown). The three different kinds of GQDs in the phosphate buffer solution (PBS) all exhibit a transparent homogeneous phase without any precipitation for at least two years (Figure 1c).

To explore the optical properties of DGG and LGG, fluorescence and circular dichroism (CD) spectroscopy were carried out. DGG and LGG have similar strong blue fluorescence (maximum 450 nm, 6% quantum yield) and their average fluorescence lifetimes were calculated to be 5.25 and 4.84 ns, respectively (Figure S4, Supporting Information). The characteristic CD peak of DGG and LGG at around 206 nm matches that in the CD spectra of free Glu (Figure 1d; Figure S5a, Supporting Information). Besides, both DGG and LGG display a new absorption band at 230–270 nm with opposite signs and similar amplitude, which might originate from the π–π^* electron transition of the sp^2-hybridized carbon network in DGG and LGG (Figure 1d; Figure S5b, Supporting Information).[18] However, no meaningful CD signal is observable for UG or racemic DL-Glu-functionalized GQD (*Rac*-GG), confirming the chiral characteristic of DGG/LGG. Meanwhile, the physical mixture of UG and D-Glu/L-Glu only shows CD absorption at 206 nm further proving that D-Glu/L-Glu is modified on DGG/LGG through chemical bonding rather than physisorption (Figure S6a, Supporting Information). The CD spectra of the Glu enantiomers after heating at 200 °C for 25 min (Figure S6b, Supporting Information) display little change compared with those of the untreated free Glu enantiomers, suggesting that the high-temperature treatment in our pyrolysis reaction does not induce condensation or configuration change of Glu[19] and therefore can be excluded as the cause of generating new CD absorption under our experimental conditions. The functional chiral Glu moiety not only preserves its own chiroptical property but also induces new chiral absorption of the sp^2-hybridized carbon structure, indicating that chirality can transfer from chiral molecule to achiral nanomaterial.[20]

The antimicrobial activities of chiral NPs were then evaluated by a standard plate count method using *Escherichia coli* and *Staphylococcus aureus* as the Gram-negative and Gram-positive model bacteria, respectively. Remarkably, DGG displayed a concentration-dependent antibacterial activity against *E. coli*. At a low concentration of 5 μg mL^{-1}, an obvious suppression effect on bacterial viability (68%) was observed for DGG. With increasing the concentrations to 10, 20, and 32 μg mL^{-1}, DGG could cause a 88%, 94%, and 99.9% decrease in bacterial viability, respectively. The dose-dependent antibacterial activity of DGG was also detected under the condition that the initial bacterial load increased to 5×10^5 colony-forming units per milliliter (Figure S7, Supporting Information).[21] In contrast, LGG and UG at concentrations of 5, 10, 20 and 32 μg mL^{-1} showed a negligible influence on the bacterial viability (**Figure 2**a,b). Similar antimicrobial activities toward *S. aureus* were also observed for DGG, LGG, and UG (Figure S8, Supporting Information). Furthermore, the Live/Dead bacterial viability assay was carried out, which

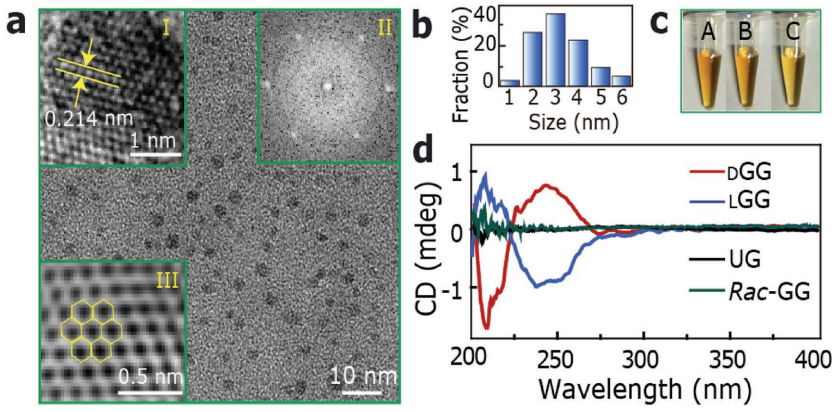

Figure 1. Characterization of chiral NPs. a) TEM images of DGG. Inset I, II, and III are the HRTEM, corresponding FFT, and reverse FFT images of DGG, respectively. b) Size distribution of DGG. c) Photographs of (A) DGG, (B) LGG, and (C) UG dissolved in PBS. d) CD spectra of DGG, LGG, UG, and *Rac*-GG. The CD resolution is 0.01 mdeg at ±200 mdeg full scale in our measuring system.

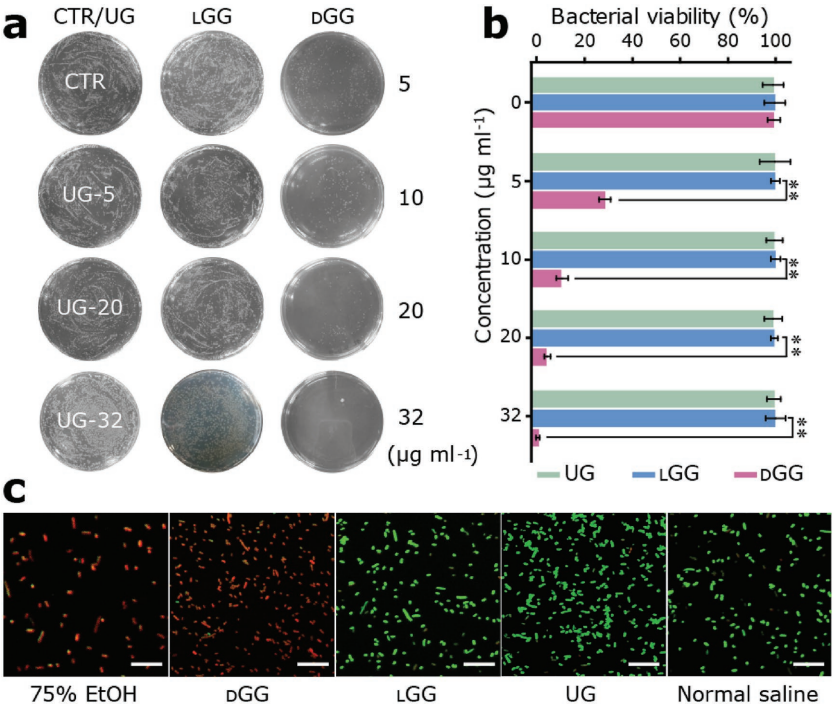

Figure 2. The antimicrobial activities of chiral NPs. a,b) Antimicrobial activities of the chiral NPs and UG against *E. coli* evaluated by a standard plate count method, $^{**}P < 0.01$. c) Live/dead fluorescence images of *E. coli* samples. Viable cells are green fluorescent and dead cells are red fluorescent. Scale bars, 10 μm. Columns and error bars represent the mean and the standard deviation, respectively, of at least three independent experiments.

can distinguish between live cells with intact membranes and dead cells with damage membranes. The result indicates that most bacteria treated with DGG (>99%) were dead, similar to the positive control treated with 75% ethanol; while the bacteria treated with LGG and UG showed a 95% survival rate which was comparable to the negative control treated with normal saline (Figure 2c). The result is well consistent with that determined by the plate count method and also demonstrates that the cell membranes are destroyed after incubation with DGG.

A good antimicrobial agent needs selective toxicity against bacteria over host cells.[22] In order to assess the cytotoxicity of chiral NPs to mammalian cells, the human cervical carcinoma epithelial cell line Hela and human neuroblastoma cell line SH-SY5Y were employed. Even at a higher concentration of 280 μg mL^{-1} (14 times of the 94% minimal inhibitory concentration), both chiral NPs and UG exhibit little influence on the growth and proliferation of Hela/SH-SY5Y cells with the viability of about 80% (Figure S9, Supporting Information), indicating their good biocompatibility. Although GQD with the assistance of irradiation or addition of H_2O_2 was reported for antibacterial application,[23] the toxicity caused by the large amount of produced reactive oxygen species compromised its biosafety in either case. Compared with other reported graphene-based NPs, such as graphene oxide (GO) and reduced GO, DGG displays much stronger antimicrobial activity and substantially lower mammalian cytotoxicity (see the Supporting Information for details).[24] In addition, considering lack of endogenously produced D-Glu and corresponding D-Glu receptor proteins in mammalian hosts, DGG hardly targets mammalian proteins to affect their functions, and therefore displays high selective toxicity toward bacteria.

To understand the cellular mechanism for the antimicrobial action of chiral NPs, we investigated the uptake of these materials into bacteria by utilizing their intrinsic fluorescence and their effects on bacterial morphology. Four groups of *E. coli* were respectively incubated with DGG, LGG, and UG at a sublethal dose (20 μg mL^{-1}) and with normal saline as the untreated control for 3 h. Then, cell membranes were stained with a red fluorescent dye FM4-64.[25] Upon excitation at 405 and 515 nm, the red fluorescence surrounds the inner blue fluorescence of chiral NPs and UG compared with the circumjacent red fluorescence of the untreatment group, demonstrating efficient internalization of all three kinds of GQDs into the bacteria (**Figure 3**a). Then, morphology changes of the bacteria were investigated by scanning electron microscopy (SEM). The *E. coli* incubated with DGG shows serious damage in the cell wall and leakage of cellular contents, while nearly all *E. coli* cells treated with LGG and UG still preserve quite complete cell wall similar to the untreated *E. coli* with smooth cell wall (Figure 3a). In addition, the leakage of cellular contents was further confirmed by quantitative analysis of the changes in the OD_{260} and OD_{280} of the bacteria suspension (Figure S10, Supporting Information). The observed severe destruction of the cell wall and cellular content leakage induced by DGG corroborates its strong antimicrobial activity.

For thoroughly understanding the antimicrobial mechanism of chiral NPs at the molecular level, the binding interaction and corresponding inhibitory effect of DGG/LGG on the D-Glu-adding enzyme—MurD ligase—were studied by microscale thermophoresis (MST) measurement, CD spectroscopy, and enzymatic activity assay. The MST result (Figure 3b) displays that the binding between DGG and the recombinant MurD protein is saturated at a relatively low concentration with an equilibrium dissociation constant of about 300×10^{-6} M. The high affinity and low capacity of the binding interaction indicate that DGG can specifically bind to MurD ligase.[26] In contrast, LGG and UG exhibit much weaker binding ability to MurD protein. Then, the protein secondary structure changes of MurD after interaction with chiral NPs were examined by CD spectroscopy. Compared with the free MurD, MurD complexed with 4×10^{-6} M of DGG displays a reduction in the CD ellipticity in the range of 200–230 nm, and a further decrease when increasing the concentration of DGG to 16×10^{-6} M (Figure 3c; Table S1, Supporting Information). While no meaningful alteration in the intensity of the characteristic CD peak was detected for MurD complexed with LGG (4×10^{-6} and 16×10^{-6} M). The significant change in the secondary structure of MurD protein indirectly confirms the strong binding interaction between DGG and MurD, and also suggests a possible inhibitory effect of

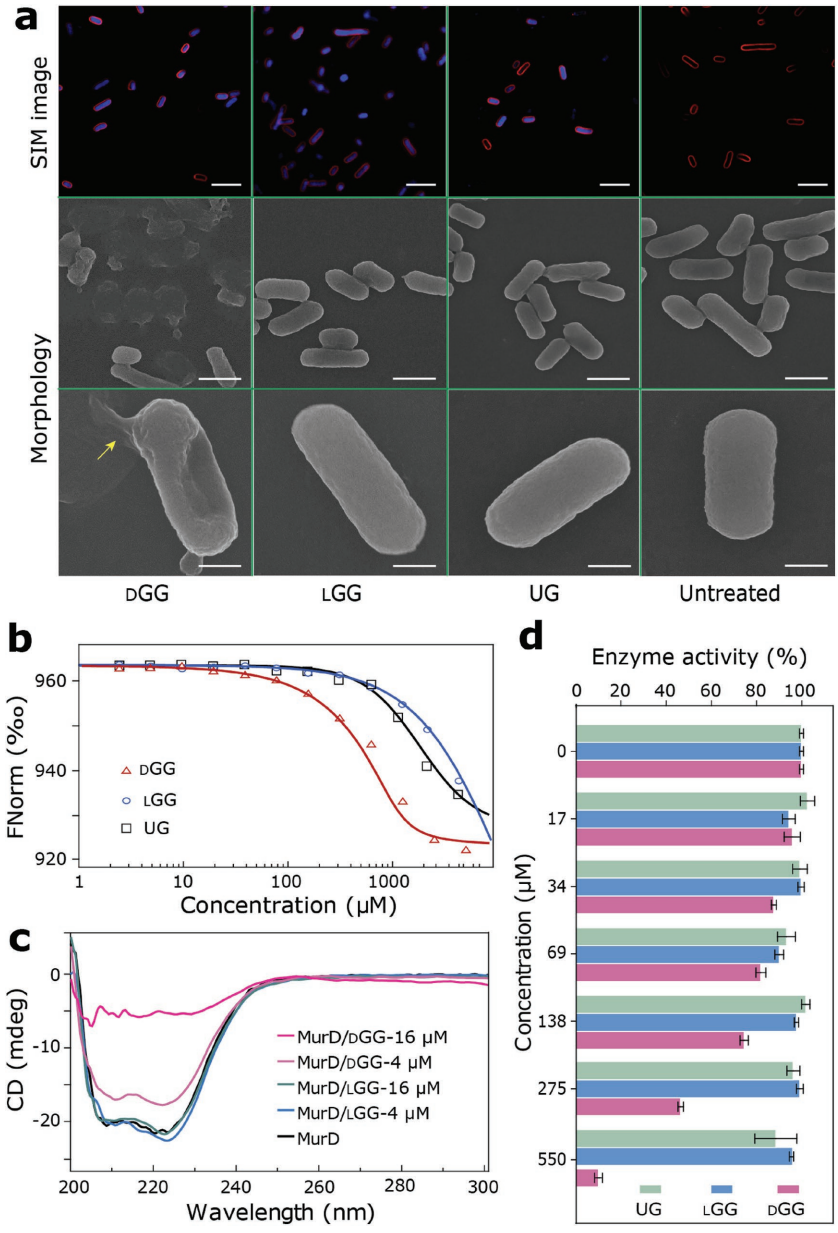

Figure 3. Antimicrobial mechanism of DGG. a) The structured illumination microscopy (SIM) and SEM images of the *E. coli* after incubated with DGG, LGG, and UG at 20 μg mL^{-1} and with normal saline as the untreated control for 3 h, respectively. Scale bars, 5 μm (SIM images in the first row), 1 μm (large-scale images in the second row), and 500 nm (zoomed-in images in the third row, and the yellow arrow indicates the leaked cellular contents). b) Binding curves derived from the specific change in the thermophoretic mobility of MurD protein upon titration with DGG, LGG, and UG, respectively. c) The far-UV CD spectra of MurD proteins after incubation with DGG and LGG (4 and 16 × 10^{-6} M), respectively, at 25 °C for 60 min. The untreated MurD protein was taken as a control. d) The relative enzymatic activity of MurD ligase after treatment with DGG, LGG, and UG at different concentrations in the range of 0–550 × 10^{-6} M. Columns and error bars represent the mean and the standard deviation, respectively. Three independent experiments were performed in triplicate.

DGG on MurD. Last, the catalyzing activity of MurD ligase after treatment with DGG was investigated to evaluate the inhibitory effect of DGG. After incubating MurD with 17 × 10^{-6}, 34 × 10^{-6}, 69 × 10^{-6}, 138 × 10^{-6}, 275 × 10^{-6}, and 550 × 10^{-6} M of DGG, its enzymatic activity was decreased by 4%, 12%, 18%, 25%, 54%, and 89%, respectively (Figure 3d). In contrast, nearly 90% of relative enzymatic activity was retained for MurD after incubation with UG or LGG at the above same concentrations, demonstrating a negligible inhibitory effect on MurD for UG and LGG. Addition of Glu to the cellular PG precursor catalyzed by MurD ligase is an essential step for intracellular PG biosynthesis, therefore, inhibition of MurD activity after binding DGG plays a predominant role in causing the destruction of cell wall by disrupting the intracellular PG biosynthesis.

The underlying mechanism of the different inhibitory effect of chiral NPs on MurD enzymatic activity was finally elucidated via molecular dynamics (MD) simulations using the simplified NP models (see the Supporting Information for details). During the 10 ns MD simulation, DGG has much larger root-mean-square deviation variation than LGG (Figure S11, Supporting Information), indicating that it has a greater change in conformation and the interactions of different chiral NPs with MurD may be different. And a considerable number of aromatic amino acids are distributed at the active site of MurD with most atoms at the active site being neutrally charged (Figure S12, Supporting Information); thus, the hydrophobic π-conjugated domain of chiral NPs can facilitate binding to such a nonpolar active site. The calculated total binding free energy (ΔG_{tot}) of the DGG/MurD complex is 3.68 kcal mol^{-1} lower than that of the L-type complex, and the driving force is found to be the van der Waals energy (**Figure 4**a; see the Supporting Information for details). It should be noted that this energy difference is quite large in a thermodynamic sense,[27] comparable to the Gibbs free energy of formation of gaseous ammonia (–3.92 kcal mol^{-1}),[28] suggesting that the binding interaction of MurD with DGG is much stronger than that with LGG.

To investigate the key amino acid residues in MurD responsible for the significant difference of ΔG_{tot} between the DGG/MurD and LGG/MurD complexes, the binding free energy decomposition was performed. The result reveals that there are six key residues contributing to this energy difference (Figure 4b). Among these residues, five residues exhibit stronger binding affinity for DGG than for LGG, and only Arg37 displays a weaker binding affinity for DGG in comparison with that for LGG (Figure S13, Supporting Information). Especially, Phe161 and Pro72 show much higher energy contributions to ΔG_{tot} of the DGG/MurD complex (–1.61 and –3.61 kcal mol^{-1}) than those to ΔG_{tot} of the

a Binding free energy (kcal mol^{-1})

Complex	ΔE_{vdw}	ΔE_{ele}	ΔG_{SA}	ΔG_{GB}	ΔG_{tot}
DGG/MurD	-51.53	21.34	-6.98	-17.90	-55.11
LGG/MurD	-48.31	21.87	-6.68	-18.31	-51.43

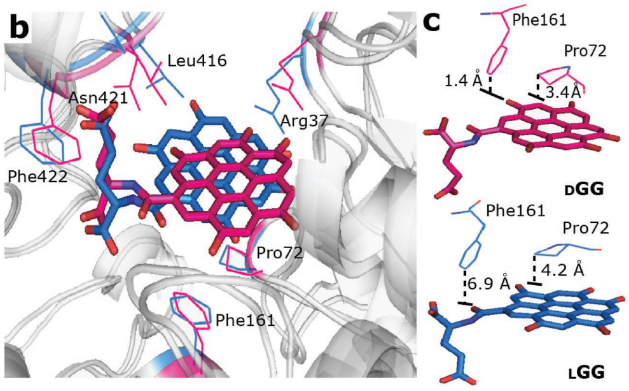

Figure 4. Different binding interactions of MurD ligase with DGG and LGG. a) Binding free energy of the DGG/MurD and LGG/MurD complexes, respectively. ΔE_{vdw} and ΔE_{ele} are the van der Waals and electrostatic energy, respectively. ΔG_{GB} corresponds to the polar desolvation free energy, while ΔG_{SA} stands for the nonpolar component of desolvation free energy. ΔG_{tot} is the calculated total binding free energy without consideration of conformational entropy. b) The key residues contributing to the difference in the total binding free energy (shown as hot pink and blue sticks in the ligand-binding sites for DGG and LGG, respectively). c) The perpendicular (T-shaped) and parallel-displaced π–π interactions between the planar π-conjugated domain of chiral NPs and Phe161 and Pro72 in MurD ligase, respectively.

L-type complex (–0.45 and –2.95 kcal mol^{-1}) through perpendicular (T-shaped) and parallel-displaced π–π interaction with the planar π-conjugated domain of chiral NPs, respectively (Figure 4c). The vertical distances from Phe161 and Pro72 to the planar π-conjugated domain in the DGG/MurD complex are respectively 1.4 and 3.4 Å, much shorter than those (6.9 and 4.2 Å, respectively) in the L-type complex, indicating that DGG is more favorable for MurD binding than its L-type counterpart. Since hydrogen bonding is an important intermolecular interaction in biological systems, a further analysis on it in the chiral NP/MurD complexes was also performed. The data of hydrogen bond occupancy reveals that the hydrogen bonding in the D-type complex is stronger than that in the L-type (see Table S2 and Figure S14 in the Supporting Information for details), showing that the stereo-configuration of Glu moiety is critically important for the selective binding interaction between chiral NPs and MurD. The above results indicate that the thermodynamic stability of DGG/MurD complex is higher than that of the L-type complex considering that DGG shows favorable stereo adaption to MurD. For our chiral NP/MurD complexes, a new chiral activity is induced in chiral NP, and the noncovalent interactions (van der Waals forces and hydrogen bonding) between MurD and two moieties of chiral NPs work together to cause the enzymatic inhibition and final antibacterial activity, which is similar to the induced chirality and synergistic effect in the chiral supramolecular system.[29] The binding of DGG to the active site of MurD can prevent the Glu substrate from binding to the same active site and thereby inhibit the enzymatic activity. Considering that the crystal structure of MurD ligase shows a flexible active cleft[30] with the size of several nanometers (Figure S11b, Supporting Information), the single-atomic-layer DGG with an average size of 3 nm is suitable for docking in the flexible cleft of MurD ligase and thus possesses potential antimicrobial activity. The current work was undertaken as a proof of concept about the influence of chirality on the antibacterial activity and its selective toxicity of the nanoparticle. Many research studies indicate that the NP size is a key parameter for its toxicity to bacteria and mammalian.[31] In addition to the size effect, the nonspecific adsorption on the surface of NPs might affect their binding interaction with the targets, and the final toxicity to bacteria and mammalian cells (Figure S15, Supporting Information). Work on systematic optimization of the NP size and surface modification is ongoing in our group to further promote the antimicrobial performance and selective toxicity of NPs.

In summary, we have developed a novel chiral biomolecule (D-Glu) functionalized GQD with effective antimicrobial activity and high selective toxicity against microorganism over mammalian cells. Our cellular level experiments show that DGG can be taken up into bacteria and cause severe damage of the cell wall, thus exerting efficient antimicrobial activity against both Gram-negative and Gram-positive bacteria, while its counterpart LGG displays negligible antimicrobial activity. Meanwhile, our molecular level experiments reveal that DGG can bind to MurD ligase and change its secondary structure, inhibit MurD from catalyzing the intracellular biosynthesis of PG, and therefore disrupt the formation of integral cell wall. Futhermore, the theoretical investigation reveals that the binding between MurD and DGG especially the van der Waals and hydrogen bonding interaction is stronger than that of LGG/MurD, which might contribute to the higher inhibitory effect of DGG. In addition, the unique presence of D-Glu and MurD protein in bacteria rather than in mammalian cells contributes to the selective toxicity of DGG toward bacteria over mammalian cells. Our deliberate and effective antimicrobial strategy provides insights for development of novel chiral antimicrobial NPs with high efficiency and excellent biosafety.

Supporting Information

Supporting Information is available from the Wiley Online Library or from the author.

Acknowledgements

Q.X., Q.L., and L.G. contributed equally to this work. The authors acknowledge the financial support from the National Natural Science Foundation of China (Grant Nos. 21573049, 21422303, and 81602643), National Key R&D Program "nanotechnology" special focus (Grant No. 2016YFA0201600), Beijing Natural Science Foundation (Grant No. 2142036), Knowledge Innovation Program and Youth Innovation Promotion Association of CAS, and the CAS Key Laboratory for Nanosystem and Hierarchical Fabrication. The authors also thank Prof. Mingjuan Ji (School of Chemistry and Chemical Engineering, University of CAS) for providing SYBYL software.

Received: September 2, 2016
Revised: November 29, 2016
Published online:

[1] a) Y. Y. Liu, Y. Wang, T. R. Walsh, L. X. Yi, R. Zhang, J. Spencer, Y. Doi, G. Tian, B. Dong, X. Huang, *Lancet Infect. Dis.* **2016**, *16*, 161; b) S. B. Levy, B. Marshall, *Nat. Med.* **2004**, *10*, S122.
[2] a) A. Sharma, D. Kumar Arya, M. Dua, G. S. Chhatwal, A. K. Johri, *Expert Opin. Drug Delivery* **2012**, *9*, 1325; b) A. J. Huh, Y. J. Kwon, *J. Controlled Release* **2011**, *156*, 128.
[3] a) S. Kang, M. Pinault, L. D. Pfefferle, M. Elimelech, *Langmuir* **2007**, *23*, 8670; b) Y. J. Tang, J. M. Ashcroft, D. Chen, G. Min, C. H. Kim, B. Murkhejee, C. Larabell, J. D. Keasling, F. F. Chen, *Nano Lett.* **2007**, *7*, 754; c) W. Hu, C. Peng, W. Luo, M. Lv, X. Li, D. Li, Q. Huang, C. Fan, *ACS Nano* **2010**, *4*, 4317; d) Y. Tu, M. Lv, P. Xiu, T. Huynh, M. Zhang, M. Castelli, Z. Liu, Q. Huang, C. Fan, H. Fang, R. Zhou, *Nat. Nanotechnol.* **2013**, *8*, 594.
[4] C. Zhu, Q. Yang, L. Liu, F. Lv, S. Li, G. Yang, S. Wang, *Adv. Mater.* **2011**, *23*, 4805.
[5] I. Irwansyah, Y. Q. Li, W. Shi, D. Qi, W. R. Leow, M. B. Tang, S. Li, X. Chen, *Adv. Mater.* **2015**, *27*, 648.
[6] a) J. He, W. Wang, F. Sun, W. Shi, D. Qi, K. Wang, R. Shi, F. Cui, C. Wang, X. Chen, *ACS Nano* **2015**, *9*, 9292; b) Z. M. Xiu, Q. B. Zhang, H. L. Puppala, V. L. Colvin, P. J. Alvarez, *Nano Lett.* **2012**, *12*, 4271; c) Y. Zhao, Y. Tian, Y. Cui, W. Liu, W. Ma, X. Jiang, *J. Am. Chem. Soc.* **2010**, *132*, 12349; d) Y. Q. Li, B. Zhu, Y. Li, W. R. Leow, R. Goh, B. Ma, E. Fong, M. Tang, X. Chen, *Angew. Chem., Int. Ed.* **2014**, *53*, 5837; e) C. M. Courtney, S. M. Goodman, J. A. McDaniel, N. E. Madinger, A. Chatterjee, P. Nagpal, *Nat. Mater.* **2016**, *15*, 529.
[7] M. J. Hajipour, K. M. Fromm, A. A. Ashkarran, D. Jimenez de Abe-rasturi, I. R. de Larramendi, T. Rojo, V. Serpooshan, W. J. Parak, M. Mahmoudi, *Trends Biotechnol.* **2012**, *30*, 499.
[8] a) K. E. Sapsford, W. R. Algar, L. Berti, K. B. Gemmill, B. J. Casey, E. Oh, M. H. Stewart, I. L. Medintz, *Chem. Rev.* **2013**, *113*, 1904; b) M. Veerapandian, K. Yun, *Appl. Microbiol. Biotechnol.* **2011**, *90*, 1655.
[9] a) M. Zhang, G. Qing, T. Sun, *Chem. Soc. Rev.* **2012**, *41*, 1972. b) B. Chang, M. Zhang, G. Qing, T. Sun, *Small* **2015**, *11*, 1097.
[10] A. L. Lovering, S. S. Safadi, N. C. Strynadka, *Annu. Rev. Biochem.* **2012**, *81*, 451.
[11] J. P. Behr, *The Lock and Key Principle*, John Wiley & Sons, New York **1994**.
[12] K. Strancar, A. Boniface, D. Blanot, S. Gobec, *Arch. Pharm.* **2007**, *340*, 127.
[13] I. Kouidmi, R. C. Levesque, C. Paradis-Bleau, *Mol. Microbiol.* **2014**, *94*, 242.
[14] R. Sink, H. Barreteau, D. Patin, D. Mengin-Lecreulx, S. Gobec, D. Blanot, *Biomol. Concepts* **2013**, *4*, 539.
[15] a) H. Sun, L. Wu, W. Wei, X. Qu, *Mater. Today* **2013**, *16*, 433; b) Q. Liu, B. Guo, Z. Rao, B. Zhang, J. R. Gong, *Nano Lett.* **2013**, *13*, 2436; c) S. Zhu, Y. Song, X. Zhao, J. Shao, J. Zhang, B. Yang, *Nano Res.* **2015**, *8*, 355; d) R. Ye, C. Xiang, J. Lin, Z. Peng, K. Huang, Z. Yan, N. P. Cook, E. L. Samuel, C. C. Hwang, G. Ruan, G. Ceriotti, A. R. Raji, A. A. Martí, J. M. Tour, *Nat. Commun.* **2013**, *4*, 2943.
[16] a) J. Peng, W. Gao, B. K. Gupta, Z. Liu, R. Romero-Aburto, L. Ge, L. Song, L. B. Alemany, X. Zhan, G. Gao, *Nano Lett.* **2012**, *12*, 844; b) P. Luo, Y. Qiu, X. Guan, L. Jiang, *Phys. Chem. Chem. Phys.* **2014**, *16*, 19011.
[17] a) Y. Dong, H. Pang, H. B. Yang, C. Guo, J. Shao, Y. Chi, C. M. Li, T. Yu, *Angew. Chem., Int. Ed.* **2013**, *52*, 7800; b) L. Wang, Y. Wang, T. Xu, H. Liao, C. Yao, Y. Liu, Z. Li, Z. Chen, D. Pan, L. Sun, M. Wu, *Nat. Commun.* **2014**, *5*, 5357.
[18] S. Zhu, Y. Song, X. Zhou, J. Shao, J. Zhang, B. Yang, *Nano Res.* **2015**, *8*, 335.
[19] H. Rong, W. Li, Z. Chen, X. Wu, *J. Phys. Chem. B*, **2008**, *112*, 1454.
[20] a) S. Ostovar pour, L. Rocks, K. Faulds, D. Graham, V. Parchansky, P. Bour, E. W. Blanch, *Nat. Chem.* **2015**, *7*, 591; b) N. Suzuki, Y. Wang, P. Elvati, Z. B. Qu, K. Kim, S. Tiang, E. Baumeister, J. Lee, B. Yeom, J. H. Bahng, J. Lee, A. Violi, N. A. Kotov, *ACS Nano* **2016**, *10*: 1744.
[21] I. Wiegand, K. Hilpert, R. E. Hancock, *Nat. Protoc.* **2008**, *3*, 163.
[22] M. Debono, R. S. Gordee, *Annu. Rev. Microbiol.* **1994**, *48*, 471.
[23] H. Sun, N. Gao, K. Dong, J. Ren, X. Qu, *ACS Nano* **2014**, *8*, 6202.
[24] a) S. Liu, T. H. Zeng, M. Hofmann, E. Burcombe, J. Wei, R. Jiang, J. Kong, Y. Chen, *ACS Nano* **2011**, *5*, 6971; b) L. Shi, J. Chen, L. Teng, L. Wang, G. Zhu, S. Liu, Z. Luo, X. Shi, Y. Wang, L. Ren, *Small* **2016**, *12*, 4165.
[25] E. A. Libby, M. Roggiani, M. Goulian, *Proc. Natl. Acad. Sci. USA* **2012**, *109*, 7445.
[26] P. M. Ray, U. Dohrmann, *Plant Physiol.* **1977**, *59*, 357.
[27] Y. Zhou, M. Yang, K. Sun, Z. Tang, N. A. Kotov, *J. Am. Chem. Soc.* **2010**, *132*, 6006.
[28] D. R. Lide, *CRC Handbook of Chemistry and Physics*, CRC Press, Boca Raton, **2004**.
[29] a) M. Liu, L. Zhang, T. Wang, *Chem. Rev.* **2015**, *115*, 7304; b) A. G. de Bruin, M. E. Barbour, W. H. Briscoe, *Polym. Int.* **2014**, *63*, 165.
[30] A. Perdih, M. Kotnik, M. Hodoscek, T. Solmajer, *Proteins: Struct., Funct., Bioinf.* **2007**, *68*, 243.
[31] a) F. Muller, T. Dégousée, J. Degrouard, A. Brûlet, A. Salonen, *J. Colloid Interface Sci.* **2015**, *446*, 114; b) M. V. Park, A. M. Neigh, J. P. Vermeulen, L. J. de la Fonteyne, H. W. Verharen, J. J. Briedé, H. van Loveren, W. H. de Jong, *Biomaterials* **2011**, *32*, 9810; c) Y. Pan, S. Neuss, A. Leifert, M. Fischler, F. Wen, U. Simon, G. Schmid, W. Brandau, W. Jahnen-Dechent, *Small* **2007**, *3*, 1941; d) A. Ivask, I. Kurvet, K. Kasemets, I. Blinova, V. Aruoja, S. Suppi, H. Vija, A. Käkinen, T. Titma, M. Heinlaan, M. Visnapuu, D. Koller, V. Kisand, A. Kahru, *PLoS One* **2014**, *9*, e102108.